

See discussions, stats, and author profiles for this publication at: <https://www.researchgate.net/publication/326699655>

Experimental investigation of effect of orientation and surface roughness on drying of porous media consisting of rods

Article in *International Journal of Multiphase Flow* · July 2018

DOI: 10.1016/j.ijmultiphaseflow.2018.07.009

CITATIONS

15

READS

64

2 authors, including:



Navneet Kumar

Indian Institute of Technology Jammu

54 PUBLICATIONS 171 CITATIONS

[SEE PROFILE](#)

Some of the authors of this publication are also working on these related projects:



Heat transport in Turbulent free and mixed convection [View project](#)



Evaporation from stagnant water bodies [View project](#)

Experimental investigation of effect of orientation and surface roughness on porous media consisting of rods

Navneet Kumar and Jaywant H Arakeri
*Department of Mechanical Engineering
Indian Institute of Science*

Abstract

Studies of drying from a conventional porous medium (CPM), consisting of spheres, have shown the existence of three periods. In the first period drying rate is high and essentially depends on the atmospheric demand while in the last stage mass transfer happens from within the porous medium and is solely governed by the internal properties. In a previous study [5] it was shown, using a cluster of closely packed smooth rods stacked vertically, that stage 1 was sustained till nearly the whole liquid gets evaporated. *Near-zero radii* contacts, between the rods, offering infinite height rise was shown to be the reason behind such high sustained evaporation rates and elongated duration of stage 1. Here we show that the orientation of the rods dramatically changes the evaporation process from a rod-based porous medium (RBPM). Unlike the vertical case, in the horizontal case (HRBPM) smooth rods do not support stage 1. In this case transition to stage 2 was not due to the films but to the liquid-vapour meniscus receding continuously in the network. Rough rods pinned the liquid along its rough surfaces and stage 1 is sustained although its duration is much smaller compared to the vertical case. Maintained hydraulic connections against gravity along the roughness of the rods thus provides a better insight towards understanding stage 1 in a conventional porous medium consisting of complicated pore geometry and their connectivity. Infra-red heating at about 1000 W/m^2 causes evaporation from an initially saturated RBPM kept in an acrylic box.

1. Introduction

Drying of a porous medium finds its application in vast majority of applications and thus has been studied extensively in field and in laboratory experiments. Although soil particles are in general irregular and non-uniform most of the laboratory studies have been from porous media made up of spheres. These spheres include both mono-disperse particles consisting glass beads [1-3], metal balls [2] etc. and poly-disperse [4] particles such as quartz sand. We term this type of porous medium consisting of 3D network of pores as conventional porous medium (CPM). A simpler void geometry can be formed if rods instead of spheres are used. We term these systems as RBPM (rods based porous medium) where two basic configurations of rods are: vertical and horizontal. Vertical (VRBPM) orientation has been recently studied [5] and a few surprising features were shown compared to CPM.

Previous studies [2-4,6,7] have shown three distinct stages of drying from a CPM; initial saturation also affects the existence of these stages [8,9]. In the 1st stage, high rates of evaporation are observed; this stage is a constant rate period (CRP) as the evaporation rate is nearly constant [4,6]. Water present near the open end of a porous medium leads to such a high evaporation rate. Near-surface water can be sustained by liquid film(s) in a porous medium; this film is the source of hydraulic connection between the near-surface water and the bulk (drying front) [3]. Nuclear-based [10-13] water content mapping has clearly shown the presence of these liquid films. In cases where films are responsible for stage 1, its breakage (depinning) [2] then leads to drastic fall in the evaporation rate and is termed transition regime or falling rate period (FRP). In the last stage i.e. stage 2, the liquid-vapour (L-V) meniscus recedes [6] from the top surface with time and is termed receding front period (RFP). The time of onset of FRP strongly depends on the average pore size [2-4]. Transition to RFP or FRP can also occur without the film break-up. For larger particles in a CPM capillary film effect is negligible [2] and in this case water moves (recedes) smoothly with time within the porous medium; with no significant formation of islands (wet) in the network apart from some of the water getting trapped in the contacts of the spheres.

Formation of vapour fingers in the centre of the capillary with imbibing liquid along the corners of a polygonal capillary is well known [14-19] and during drying a combination of these networks [20] was shown to sustain stage 1 numerically. These features are very different than a circular cross section capillary and during drying experiments capillary films formation was nicely shown [21-22] along the corners of polygonal capillaries. In the vertical case [21,22] transition to 2nd stage was observed due to depinning of the liquid to a lower location away from the open end of the square capillary. In the horizontal case [23] the transition did not occur due to depinning but rather due to change in the corner menisci geometry. These pinned liquid films were able to sustain high mass transfer, similar to stage 1 in CPM, compared to circular capillaries which was first observed [24] in horizontal nanochannels. An extreme case of a polygonal capillary was recently studied [5] where rods were stacked vertically (against gravity) in a closed packed structure. Note that a unit cell in such a study consists of three rods in mutual

contact. The unit pore in RBPM is the straight region formed by three circular arcs formed by three rods in contact with each other. The void in this case thus has three corners with “*near-zero radii* [5]” which can also be thought of polygonal capillary with zero internal angles. Limitless capillary rise [25,26] can happen along these corners and forced depinning length was reported during the drying [5].

Features of a CPM during its drying are nicely covered in a recent article [27]. Aim of the current study, though, is to investigate the effect of orientation in drying of a RBPM where corners dominate the whole process. We focus mostly on the characteristics of horizontal orientation and its differences with respect to the vertical orientation. This basic configuration was studied [28] previously during capillary rise where gravity was not important. Using the experimental observations during the drying process we show that this configuration can be used effectively in reducing evaporation and can also be treated as a base case of transition to stage 2 without any significant film effect. Further we show the effect of rods surface roughness on drying from the two configurations. Note that even for smooth rods the contact will be limited to the roughness scales throughout their lengths.

2. Experimental methodology

Experiments with horizontally stacked rods were conducted with an acrylic box having a height of 40 mm and 76 mm x 50 mm as the cross-sectional dimensions. Circular cross-section rods (2 mm & 3 mm diameter glass and 0.7 mm diameter pencil rods) were stacked in the acrylic box; the length of the rods was 75 mm. Experiments with vertically stacked rods were conducted with a different acrylic box having a height of 78 mm and 51 mm x 41 mm as the cross-sectional dimensions. The box was filled with water till its brim and initially a single layer of rods were placed at the container bottom. Rods were then placed on top of the bottom most layer to obtain a HRBPM. Such porous media are seen in Figure 1(a) and (b) for 0.7 mm diameter pencil rods and 3.0 mm diameter glass rods respectively; rods are exposed length-wise. Note that during the packing of rods water gets expelled corresponding to the added rods volume. Excess water was then removed to obtain the saturated mass of water in HRBPM. Finally in all the experiments a thin (2-3 mm) layer of liquid was added on top of initially saturated HRBPM, which enabled us to obtain, as reference, the evaporation rate from a bare water surface. For comparison vertically stacked rod-based porous medium (VRBPM) consisting of 0.7 mm diameter pencil rods are seen in Figure 1(c) and (d); rods diameter portion is exposed to the ambient.

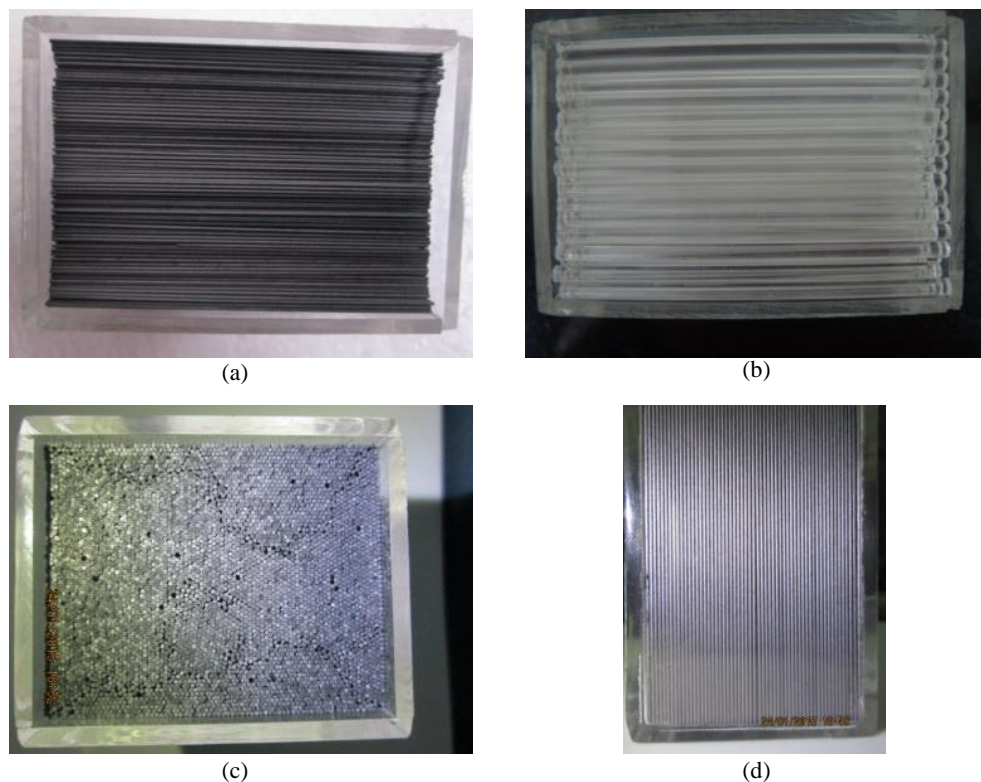


Figure 1 Pictures showing the top view of HRBPM with (a) 0.7 mm diameter pencil rods and (b) 3.0 mm diameter glass rods. Top (c) and side (d) view of VRBPM consisting of 0.7 mm diameter pencil rods.

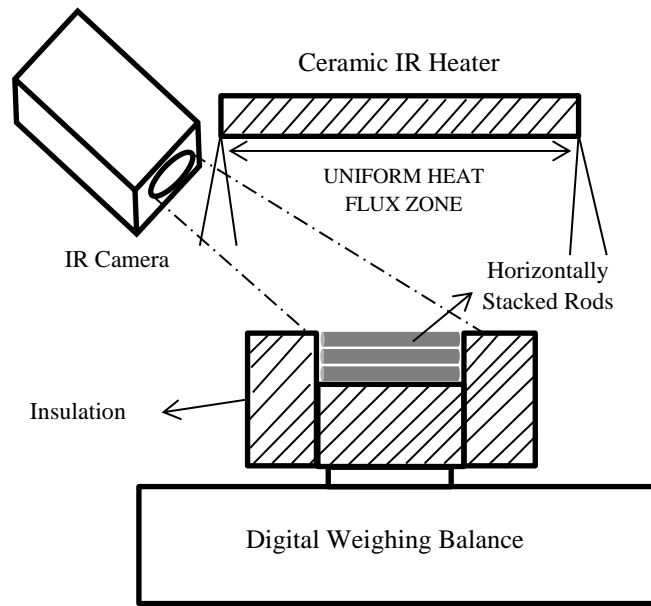


Figure 2 Schematic of the experimental setup. Rods are shown stacked horizontally.

Figure 2 shows the experimental setup and remain similar to previous studies [2,5]. Evaporation from the porous medium was due to infrared (IR) heating from the top. Mass loss was measured using a precision weighing balance (Sartorius GPA5202). An IR camera (Fluke Ti400) measures the top surface temperature of the porous medium and a T-type thermocouple was used to measure the temperature of the bottom (outer) surface of the acrylic box. To minimize heat loss, the acrylic box was insulated on the four sides and the bottom. Recently [29-32] IR camera has been used to great effect in obtaining the surface energy budget of porous media.

Material (mm), Dia. (mm), Orientation	Saturated Mass (g)	Exp. ϕ (%)	Theor. ϕ (%)
Glass Rods (GRH) 2.0, Horizontal	30.36	19.97	15.33
Glass Rods (GRH) 3.0, Horizontal	28.80	17.18	15.17
Pencil Rods (PRH) 0.7, Horizontal	28.75	21.13	12.42
Glass Rods (GRV) 2.0, Vertical	29.41	18.88	15.26
Glass Rods (GRV) 3, Vertical	28.29	18.05	16.16
Pencil Rods (PRV) 0.7, Vertical	18.56	12.63	11.82

Table 1 List of values used in the study of HRBPM containing rods; ϕ represents the volume porosity. Also listed are experimental values for VRBPM cases.

The theoretical porosity value for an infinite array of closely packed circular rods is 9.31%. Based on the measured mass of water at (near) saturation we obtained the porosity values for all the cases listed in Table 1. Also listed are the theoretical porosity values accounting for the boundary effect of the planar walls. The difference between the theoretical and experimental values in porosity is mainly due to presence of defects away from the wall and boundary regions where a close packed structure is impossible. A slightly higher experimental porosity value for the pencil rods is due to its lower density compared to the glass rods. Experiment with a different fluid less dense than water such as n-pentane is expected to reduce the porosity value. Note that, in comparison, the porosity value for packed spheres is much higher and ranges between 31% and 45%.

3. Results and discussion

The raw mass loss data measured using the scale is converted to get the evaporation rate; expressed in the units of ‘mm/d’. We first discuss the evaporation characteristics of a HRBPM and compare it with that of a VRBPM; both consisting of 2 mm diameter smooth glass rods. Note that the exposed (to the ambient) regions are the diameter and length sides in VRBPM and HRBPM respectively. For both the experiments excess water (~5g or 2.4 mm for vertical i.e. GRV case and ~7g or 1.8 mm for horizontal case i.e. GRH case) was put on top of the saturated porous media.

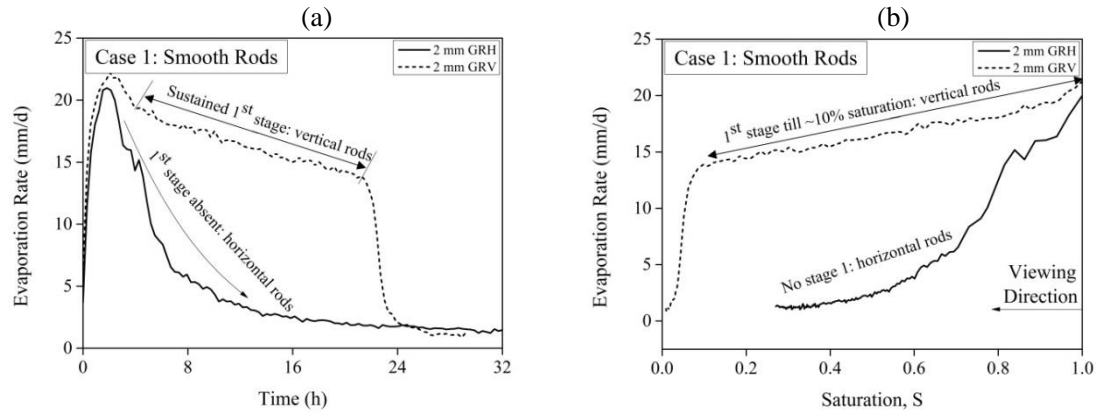


Figure 3 Experimental data for the two orientations of RBPM consisting of smooth 2 mm diameter glass rods showing (a) evaporation rate versus time and (b) evaporation rate versus saturation.

Variation with time of the evaporation rate is seen in Figure 3(a). In the presence of IR heating the evaporation rate is seen increasing. It reaches a maximum (~20 mm/d) value soon. Excess water is evaporated in nearly 2.44h and 2.95h for GRH and GRV cases respectively. Note that the initial distance between the surface and heater was 18.5 cm and when excess water evaporates completely the heat flux reaching the rods top surface reduces slightly. Once the rods are exposed higher evaporation rate (stage 1) is sustained for GRV case as seen in Figure 3(a); near-zero radii of contacts between the rods act as capillary films which source water from deeper regions to the exposed top surface. However in GRH case the rate of evaporation reduces considerably, compared to GRV case, and stage 1 lasts only till the top layer of rods are wet. Near-zero radii contacts (in GRH case) transport water horizontally (and not vertically as in GRV case) in GRH case and thus hydraulic connectivity is not maintained around the rods outer surfaces which results in unavailability of water near the top surface; stage 1 is therefore absent. Transition to stage 2 is sudden in GRV case while a gradual transition is seen for GRH case. In GRV transition is due to depinning of water films while such depinning has no meaning in GRH case. We see that a simple orientation (rods stacked horizontally) inhibits the hydraulic connectivity to such an extent that films can no longer form resulting in a classic transition to stage 2; in relation to CPM. Note that instead of length, if the rods diameter region is exposed we will always get stage 1 irrespective of the orientation i.e. GRV with top exposed is equivalent to GRH with side exposed.

Instead of time, evaporation rate is plotted versus saturation (S), ratio of instantaneous mass of water and initial saturated mass of water, as seen in Figure 3(b). The figure should be viewed from right to left as mentioned. At S=1 evaporation rate is nearly 20 mm/d for both cases. Stage 1 is sustained for GRV case till about S=0.10 while in GRH case stage 1 is very short. Consider the top layer of rods, between S = 1 to 0.8, in GRH case. The contacts (of rods with other rods) exposed to the ambient are wet while the ambient air enter from the sides (between the rods and side walls) and invades the void (between rods on top and just below it). Since the film exposed to the ambient is connected through the bulk meniscus (between three horizontal rods) stage 1 exists. Once the bulk region is completely occupied by the gas phase the top layer of rods become dry and thus stage 1 lasts for a very short time since there is no communication between the voids formed by the rods in upper layers and in lower regions. Clearly, due to lack of any significant film formation, against gravity, in GRH case the transition to stage 2 is gradual and water, almost everywhere, recedes uniformly within the network.

It is worthwhile to look at the temperature evolution of the porous medium top surface in both the cases. It has been shown earlier [2] that in presence of external heat load IR camera clearly captures the wet and dry regions on (or near) the surface; for a CPM. As long as stage 1 is sustained the top surface temperature is low and during stage 2 it increases to a much higher value [2]. IR images for the two present cases (GRH & GRV) are seen in Figure 4; three different instants are chosen for analysis. Ascending order

of temperature is seen by colours as: purple < blue < cyan < green < yellow < orange < red. Colour not in this range is out of the temperature scale as seen on the right of each IR image. Note that the colour bar is dynamic i.e. they represent different temperatures at different times but the order remains same. For both the cases at near saturation ($S \sim 1$) majority of the surface is occupied by the colder regions as seen in Figure 4(a) and (d) for GRH and GRV respectively; but slightly higher temperature is seen for GRH case owing to its lower evaporation rate (17 mm/d) compared to 20 mm/d for GRV case. At a later time, $t \sim 6$ h, evaporation rates are nearly 9 mm/d and 18 mm/d for the GRH and GRV cases respectively. Due to reduced evaporation rate in GRH case its surface temperature is higher, about 10°C , (Figure 4(b)) compared to GRV case (Figure 4(d)). Low temperature regions is limited to a few rods at this instant for GRH case as seen in Figure 4(b) which tells us that no significant film is formed here. At $t \sim 20$ h, evaporation rates are nearly 2 mm/d and 14 mm/d for the GRH and GRV cases. Note that at his instant $S = 0.46$ and 0.15 respectively for the two cases. As expected the surface temperature is much higher in case of GRH (Figure 4(e)). IR images thus clearly showed significant differences if the rod orientation is changed.

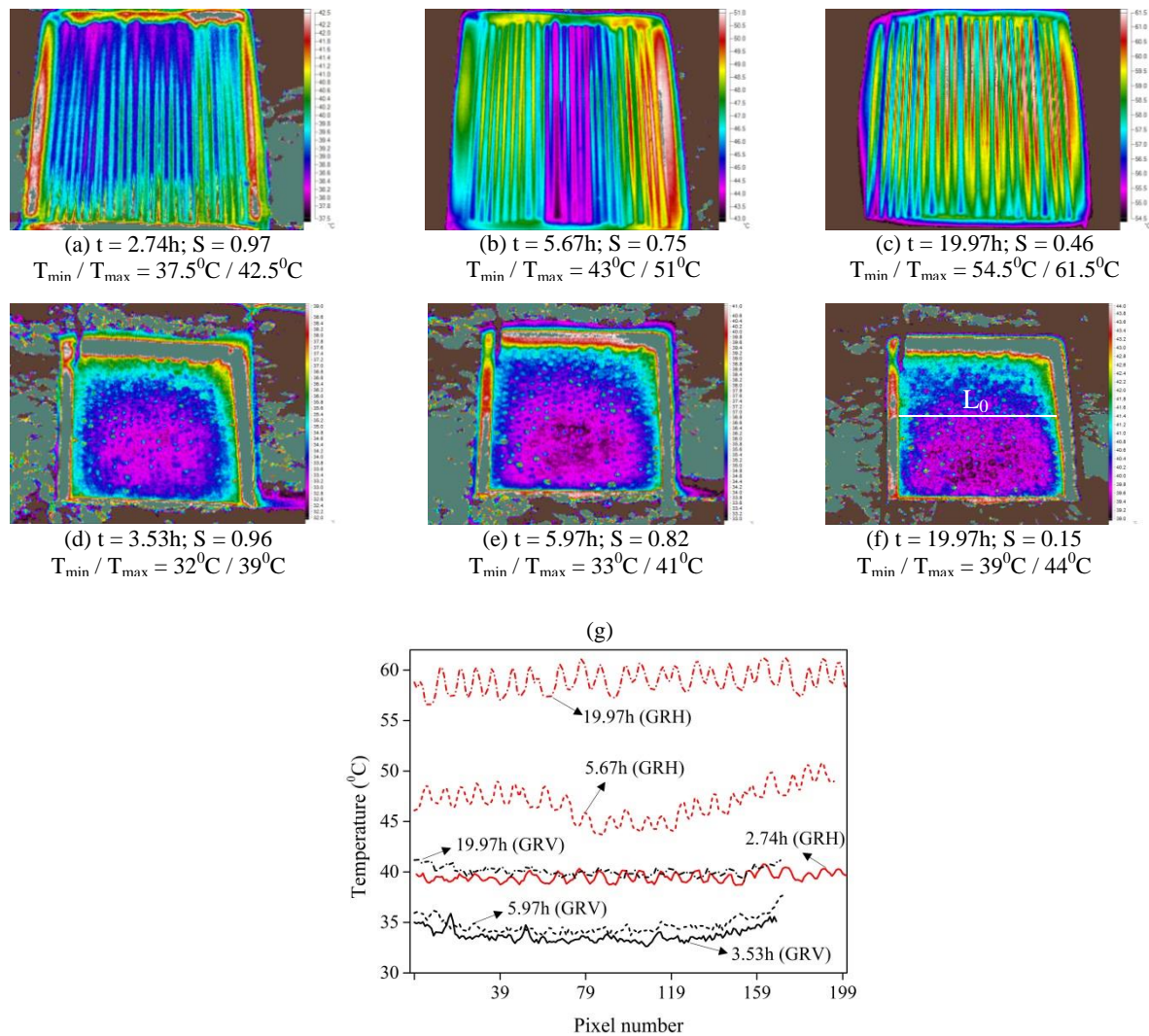


Figure 4 IR images of the top surface of the two porous media: (a-c) horizontal and (d-f) vertical case respectively. Variation, along a horizontal line (see (f)), of temperature is plotted is shown in (g). Temperature data to be seen from left to right.

Another way to look into the temperature evolution is to see its variation away from the wall. A white line (marked “ L_0 ”) is seen in Figure 4(f). Temperature along this line is plotted versus the pixel number as seen in Figure 4(g) for all the six IR images. In the absence of stage 1 temperature of GRH case is seen increasing rapidly and eclipses the temperature of GRV case quickly. Unlike GRH, temperature is seen much lower for GRV case since it is still in stage 1 (higher evaporation rate regime). For example: at $t \sim 20$ h, surface temperatures are nearly 41°C and 59°C for GRV and GRH cases respectively. Waviness profile in case of GRH is due to the rods curvature. IR camera angle changes if we move along the curve

which changed the measured temperature probably. However slight changes in the heat transfer could also have affected its temperature locally which is captured by IR camera. Note that the IR images were taken by blocking the IR radiation from the heater for a few seconds. This assured that reflected IR radiation from the porous medium surface did not enter the IR camera and gave the true temperature value.

We now discuss the effect of rods surface roughness in determining the evaporative characteristics. Surface of the glass (2 mm diameter) and pencil (0.7 mm diameter) rods are seen in Figure 5(a) and (b) respectively. It is clear that the pencil rod is rough (of the order of $10\ \mu\text{m}$) while the glass rod is very smooth. We show that, in the horizontal orientation, hydraulic connectivity can be maintained along these rough grooves around the rod leading to stage 1 which is not present in case of smooth rods.

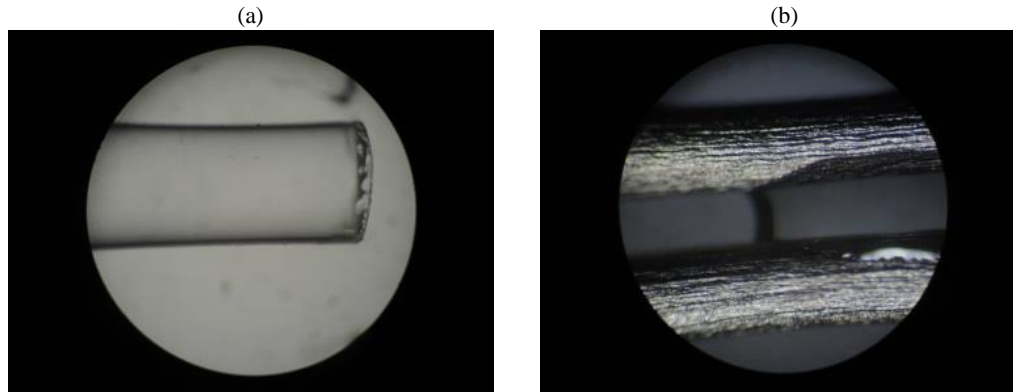


Figure 5 Pictures showing 2 mm diameter smooth glass (a) and 0.7 mm diameter rough pencil (b) rods respectively.

Evaporation rate is plotted against saturation for the pencil (PRH) and glass rods (GRH) as seen in Figure 6(a). For comparison the curve for vertically oriented pencil rods (PRV) is also shown. We see that unlike the smooth rods (GRH) stage 1 is sustained in PRH till a saturation of about 50%. The evaporation rates in stage 1 are higher than GRH case but lower than PRV case. If we assume that the hydraulic connectivity is maintained in PRH case then water between the rods will essentially be present as thin films throughout the rod length. This configuration thereby translates to evaporation from a 2D periodic array of line sources, similar to a previous [33] numerical study, separated by a distance equal to rod diameter. Note that evaporation in PRV (or GRV) cases will be 3D as it happens from point sources [34] rather than line sources. Higher evaporation rate in stage 1 in case of PRV is due to 3D nature of equiconcentration (vapour shells [35-37]) lines supporting slightly higher evaporation rates compared to the PRH case. The instant of transition to stage 2 in PRH is not quite clear at this instant. Further it would be interesting to study the effect of (order of) roughness in determining the duration of stage 1. However one thing is clear that in horizontal orientation with exposed rod lengths, very smooth rods do not exhibit any film formation around it but rougher rods do support film formation. In a CPM, stage 1 is sustained not only by the pore geometry locally and the nature of contacts therein but it's the roughness levels on the outer surfaces of spheres which connects the pores hydraulically. We have seen that similar hydraulic connections can be achieved easily using rods with rough outer surfaces. This argument makes sense since in case of very smooth outer surfaces film(s) ceases to exist due to lack of pinning locations.

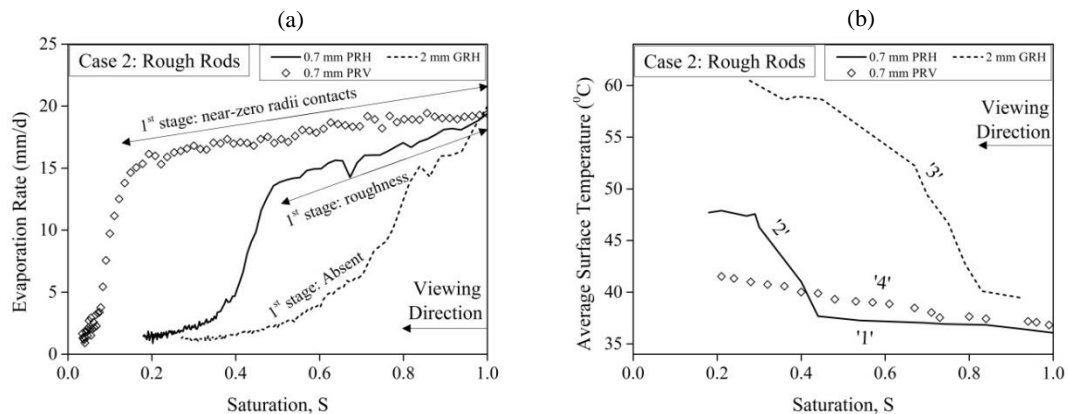


Figure 6 Variation of evaporation rates (a) and average surface temperature (b) with saturation. Also shown is the curve for pencil rods stacked vertically. In all the cases heat flux received by the top surface was about $1000\ \text{W/m}^2$.

We now discuss the surface temperature evolution for the present case; externally heated from above or non-isothermal case. The heater supplies heat to the exposed surfaces of the rods which then gets conducted, through the rods, to the L-V menisci. A part of this heat is lost into evaporation (latent heat) while the rest is used in rising (sensible heat) the temperature of the system. Since it is the top (exposed) surface which is responsible for all the exchanges (mass and heat) we should study the surface temperature evolution in detail to understand the whole process. The surface temperature is obtained by the IR images by taking the average throughout the exposed surface. For averaging a large ‘window’ (approximately 200x200 pixels) was chosen in all the IR images consisting of nearly 40,000 temperature points. Note that the resolution of the IR camera is 320x240 pixels where each pixel represents a point temperature. Temperature variations in this window are nearly $\pm 2^{\circ}\text{C}$ corresponding to the drained and evaporating zones. We use the average surface temperature as an evaporation diagnostics. Figure 6(b) shows the variation of the average surface temperature versus the saturation. For PRH case two zones are seen. Zone ‘1’ represents stage 1 where temperature increases slowly and zone ‘2’ represents the transition regime. In stage 1 the evaporation rate (see Figure 6(a)) and thus latent heat loss reduces gradually. Since the process is in near-steady state the total heat received by the surface must be lost. This is possible if the surface temperature rises which increases the convective and radiative heat losses thereby maintaining the latent heat deficit. Note that for the case of PRV a similar trend (‘4’) is seen in stage 1 although this trend will last till nearly $S=0.1$. For the GRH case stage 1 doesn’t exist and the zone with a slow temperature rise is not seen. Rapid increase in temperature with decreasing S is seen in this case (marked ‘3’ in Figure 6(b)). Note that the trend of ‘3’ in GRH case is very similar to ‘2’; transition regime of PRH case. This behaviour suggests clearly that in case of smooth rods (GRH) stage 1 is absent. The reduction in evaporation rates in stage 1 for PRV and PRH cases are slightly different as seen in Figure 6(a) which must have affected the surface temperatures. However the changes in the surface temperatures corresponding to this little difference in the evaporation rates is small and falls within the accuracy of the IR camera. In stage 2 the surface attains a much higher value as seen in Figure 6(b).

Modelling evaporation based on surface temperature

After the top layers become dry in case of smooth rods we have seen that the evaporation rate reduces due to lack of any significant film formation leading to very short stage 1. L-V menisci formed within the porous medium can be safely assumed to be relatively flatter; similar to a water surface. The menisci receive heat required for evaporation through conduction via the dry rods from the top. Based on the surface temperature of the porous medium we can predict the evaporation rate in this case. In the steady state the incoming heat will be lost completely and thus we can write the surface energy balance for the top surface as:

$$I_{total} = I_{conv} + I_{rad} + I_{ref} + I_{cond}^{surf} \quad (1)$$

Where I_{total} is the total incident IR heat flux (in W/m^2) on the top surface which gets distributed into convective heat loss (I_{conv}), radiative heat loss (I_{rad}), reflected heat (I_{ref}), and heat conducted from the surface into the porous medium (I_{cond}^{surf}). The measured surface and the ambient temperatures are used to get:

$$I_{conv} = h(T_s - T_a); I_{rad} = \sigma\epsilon(T_s^4 - T_a^4) \quad (2)$$

Where T_s and T_a are the average surface and ambient temperatures respectively, σ is the Stefan-Boltzmann constant, ϵ is the emissivity of the rods. h is the convective heat transfer coefficient which can be estimated using the Nu - Ra correlations. Ra is defined as:

$$Ra = \frac{g \left[\frac{(T_s - T_a)}{0.5(T_s + T_a)} \right] L^*{}^3}{\nu\alpha}; L^* = \frac{Area}{Perimeter} \quad (3)$$

Where g is the gravitational acceleration, L^* is a characteristic length defined as the ratio of area to the perimeter of the exposed horizontal surface, ν and α are the kinematic and thermal diffusivities of air respectively. Note that density difference, required for the natural convection, is mainly due to the temperature difference while the contribution of water vapours is relatively small and thus is neglected. For the present geometry and the incident heat flux we estimated that $Ra < 10^4$ and thus we can use the following relation to get Nu :

$$Nu = 0.59Ra^{0.25} = \frac{hL^*}{k} \quad [38] \quad (4)$$

Where k is the thermal conductivity of air. Equation (4) is used to estimate h and I_{conv} according to equation (2); Table 2 shows the range of parameters used. For the calculation of Ra the change in values of the fluid (air) properties are assumed not to change with the average fluid temperature which is indeed correct to the first order of approximation since the temperature range is not high.

T_s ($^{\circ}\text{C}$)	T_a ($^{\circ}\text{C}$)	Ra	Nu	h
41 – 61	26.5 – 27.5	1600 – 4000	3.8 – 4.7	8.8 – 11

Table 2 Range of parameters for estimating the convective heat loss from the porous medium top surface to the ambient.

The conducted heat from the surface into the porous medium can be further written as:

$$I_{cond}^{surf} = I_{cond}^{bottom} + I_{leak} + I_{sens} + I_{lat} \quad (5)$$

Where I_{cond}^{bottom} is the heat conducted from the L-V menisci to the porous medium within, I_{leak} is the heat leak through the insulation, I_{sens} is used up in heating the porous medium sensibly (heat stored), and I_{lat} is the latent heat loss term. We estimated that I_{leak} and I_{sens} is nearly 10% and 5% of I_{total} respectively. Further considering an emissivity of 0.92 for the glass rods we get the reflectivity as 8% of I_{total} ; transmissivity is assumed to be 0 for IR radiations. Equation (5) combined with equation (1) can thus be rewritten as:

$$I_{lat} = I_{total} - (I_{conv} + I_{rad}) - (I_{ref} + I_{leak} + I_{sens} + I_{cond}^{bottom}) \quad (6)$$

Nearly 10% of the incident heat flux is conducted to the bottom and we can further assume

$$I_{cond}^{bottom} = 0.1 I_{total} \quad (7)$$

Using various estimates and equation (7) we, equation (6) becomes

$$I_{lat} = 0.67I_{total} - (I_{conv} + I_{rad}) \quad (8)$$

The evaporation rate (E) is related to I_{lat} by

$$E \text{ (mm/d)} = 86.4I_{lat}/\lambda \quad (9)$$

Where λ is the latent heat of vaporization (2260 J/g). In a previous study [5] we estimated I_{total} to be about 1000 W/m^2 . We use the same value of incident heat flux since the distance between the rod's top surface and the IR heater remained same as before [5].

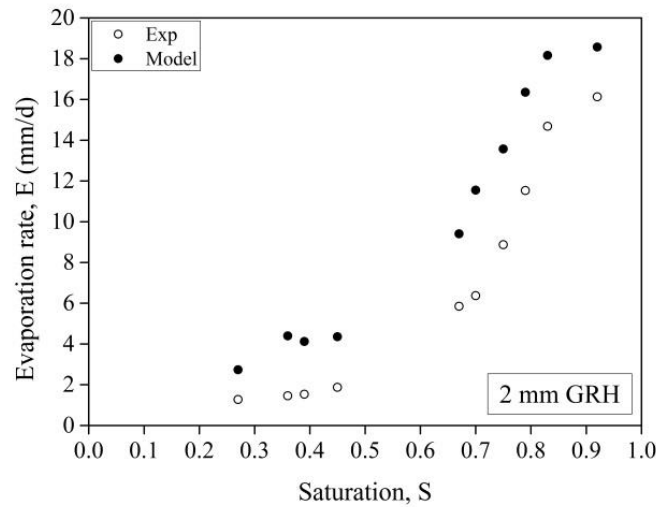


Figure 7 Estimated evaporation rates from the model (●) at different saturation values according to equations (8) and (9). Also shown are the experimentally (○) found evaporation rates.

The evaporation rates are estimated from equations (8) and (9) at the instances where IR images were captured. At these values of S the estimated evaporation rates from the model are compared with the experimental values as seen in Figure 7. Model predicted slightly higher values of E than the experimental counterpart but the trend is nicely captured. If we consider the lower bound in estimating I_{total} and take the upper bounds in estimating the other heat losses, rates from the model becomes nearly equal to the experimental values. A complete model requires the solution of the 1D heat conduction equation at the L-V menisci incorporating the thin film evaporation near the solid boundary. It essentially is an extension of the Stefan's problem with an added effect of temperature gradients within the dry and wet regions of the porous medium. A complete evaporation model is thus complex. However, the presented model captures the essential features of evaporation from stack of horizontal rods quite nicely.

Present experiments are compared with spheres-based porous media (CPM). Interest lies in the similarities or differences exhibited by the rods with its orientations when compared to the spheres. Saturation values are not good as a comparison tool since they depend on the height of the porous column. Better is to use a physical length scale such as (theoretical) average depth of water in the porous media measured from top (H_{water}) which is calculated as:

$$H_{water} = \frac{\text{Total evaporated mass}}{\text{Column height} * \phi} \quad (10)$$

Rate of evaporation for different types of porous media are plotted versus H_{water} in Figure 8. Irrespective of rods diameter (solid dashed lines) high evaporation rate is maintained till $H_{water} \sim 70$ mm for vertical cases. Transition to stage 2 weakly depends in this case. In CPM, however, transition strongly depends on the particle diameter. At the end of stage 1, $H_{water} \sim 30$ mm and 12 mm for 2.5-3.0 mm and 0.70-0.85 mm diameter glass beads respectively. Horizontally stacked rough rods sustained stage 1 till $H_{water} \sim 19$ mm. Decrease in the evaporation rate during stage 1 is steeper than the vertical cases while transition to stage 2 is still rapid. For smooth rods in horizontal orientation transition is observed from the very beginning followed soon by stage 2. The transition in this case is not rapid but a gradual one, similar to that in spheres cases.

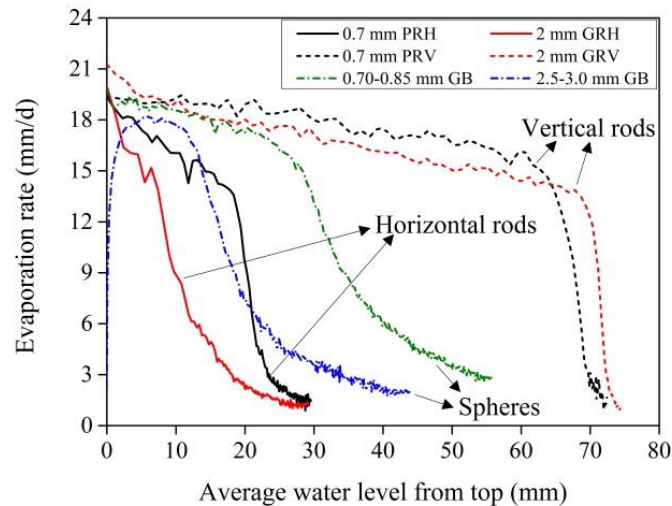


Figure 8 [Colour online] Variation of evaporation rate versus the average depth of water in different types of porous media. Data for vertical rods and spheres are also shown for comparison.

4. Conclusion

Drying characteristics of porous medium consisting of rods, stacked horizontally, have been studied and compared with that of vertically stacked rods and spheres. In the vertical orientation with diameter side exposed, the porous medium sustained high evaporation rates. Water depth till which this high evaporation rate is sustained was unusually high when compared to similarly sized spheres. This is possible due to the near-zero radii contacts transporting water all the way to the top (against gravity) where evaporation occurs.

The near-zero radii contacts transport water in the horizontal orientation, with length side exposed, also but not against the gravity. Due to this reason in case of the porous medium consisting of smooth rods stage 1 lasts till the top most voids are wet. Stage 1 is thus very short and the evaporation regime directly entered into transition followed by stage 2. The gradually reducing evaporation rate in smooth rods case was very similar to the one found in the spheres cases. Surprisingly if the rods are rough stage 1 was clearly sustained even if the rods are horizontally stacked and preferential hydraulic connectivity is along the rod lengths.

Rough rods produced enough hydraulic connectivity, around the rods, against the gravity in order to sustain stage 1. This property of rough rods is very similar to the concept of capillary film formation in case of spheres where the film path is highly tortuous due to curvilinear paths around the spheres. Roughness of the rods in vertical cases was found not to alter the evaporative characteristics. However it is surprising that changing the same configuration from vertical to horizontal brings such a major change in the properties of the porous medium. For other purposes the scale of the roughness can be controlled depending on the temporal evaporative demand. Change in the roughness values of same diameter rods would be an interesting addition to this work.

The energy required for evaporation in case of smooth rods comes from conduction via the top surface and thus essentially is a 1D heat conduction problem. A simple energy balance for the porous medium top surface augmented with the evaporation from L-V menisci within the porous medium predicted the evaporation rate quite successfully. A complete model should solve the Stefan's problem (moving interface) with the energy equation. We would also need to consider the resistance offered by the dry rods to the escaping vapours.

Acknowledgements

We gratefully acknowledge funding by Robert Bosch Centre for Cyber Physical System under the grant RBCCPS/ME/JHA/PC-0013. We also thank financial assistance provided by Indian Space Research Organization under the grant ISTC/MME/JHA/374.

References

- [1] T. M. Shaw, Drying as an immiscible displacement process with fluid counterflow, *Phys. Rev. Lett.* 59.15, (1987) 1671.
- [2] N. Kumar and J. H. Arakeri, Evaporation from confined porous media due to controlled IR heating from above, under consideration for publication in *Transport in Porous Media*.
- [3] A. G. Yiotis, D. Salin, E. S. Tajar, and Y. C. Yortsos, Drying in porous media with gravity-stabilized fronts: Experimental results, *Phys. Rev. E*, 86.2, (2012) 026310.
- [4] P. Lehmann, S. Assouline, and D. Or, Characteristic lengths affecting evaporative drying of porous media, *Phys. Rev. E*, 77.5, (2008) 056309.
- [5] N. Kumar and J. H. Arakeri, Sustained high evaporation rates from porous media consisting of packed circular rods, under consideration for publication in *Int. J. of Therm. Sci.*
- [6] T. K. Sherwood, The drying of solids—II, *Industrial & Engineering Chemistry*, 21.10 (1929) 976-980.
- [7] S. B. Idso, R. J. Reginato, R. D. Jackson, B. A. Kimball, and F. S. Nakayama, The three stages of drying of a field soil, *Soil Science Society of America Journal*, 38.5 (1974) 831-837.
- [8] J. C. Hide, Observations on factors influencing the evaporation of soil moisture, *Soil Science Society of America Journal*, 18.3 (1954) 234-239.
- [9] R. D. Jackson, B. A. Kimball, R. J. Reginato, and F. S. Nakayama, Diurnal soil-water evaporation: Time-depth-flux patterns, *Soil Science Society of America Journal*, 37.4 (1973) 505-509.
- [10] L. Pel, A. A. J. Ketelaars, O. C. G. Adan, and A. A. Van Well, Determination of moisture diffusivity in porous media using scanning neutron radiography, *International Journal of Heat and Mass Transfer*, 36(5), (1993) 1261-1267.
- [11] A. A. J. Ketelaars, L. Pel, W. J. Coumans, and P. J. A. M. Kerkhof, Drying kinetics: a comparison of diffusion coefficients from moisture concentration profiles and drying curves, *Chemical engineering science*, 50(7), (1995) 1187-1191.
- [12] R. M. E. Valckenborg, L. Pel, K. Hazrati, K. Kopinga, and J. Marchand, Pore water distribution in mortar during drying as determined by NMR, *Materials and Structures*, 34(10), (2001) 599-604.
- [13] N. Shokri, P. Lehmann, P. Vontobel, and D. Or, Drying front and water content dynamics during evaporation from sand delineated by neutron radiography, *Water Resources Research*, 44(6), (2008).
- [14] A. K. Singhal and W. H. Somerton, Two-phase flow through a non-circular capillary at low Reynolds numbers, *Journal of Canadian Petroleum Technology*, 9.03, (1970).
- [15] T. C. Ransohoff and C. J. Radke, Laminar flow of a wetting liquid along the corners of a predominantly gas-occupied noncircular pore, *Journal of Colloid and Interface Science*, 121.2, (1988) 392.

- [16] M. Dong and I. Chatzis, The imbibition and flow of a wetting liquid along the corners of a square capillary tube, *Journal of colloid and interface science*, 172.2, (1995) 278.
- [17] R. Lenormand, C. Zarcone, and A. Sarr, Mechanisms of the displacement of one fluid by another in a network of capillary ducts, *Journal of Fluid Mechanics*, 135, (1983) 337.
- [18] R. Lenormand and C. Zarcone, Role of roughness and edges during imbibition in square capillaries, SPE annual technical conference and exhibition, Society of Petroleum Engineers, (1984).
- [19] R. Lenormand, Liquids in porous media, *Journal of Physics: Condensed Matter*, 2.S, SA79 (1990).
- [20] A. G. Yiotis, A. G. Boudouvis, A. K. Stubos, I. N. Tsimpanogiannis, and Y. C. Yortsos, Effect of liquid films on the isothermal drying of porous media, *Phys. Rev. E*, 68, (2003) 037303.
- [21] F. Chauvet, P. Duru, S. Geoffroy, and M. Prat, M, Three periods of drying of a single square capillary tube, *Phys. Rev. Lett.*, 103.12, (2009) 124502.
- [22] F. Chauvet, P. Duru, and M. Prat, Depinning of evaporating liquid films in square capillary tubes: Influence of corners' roundedness, *Physics of Fluids*, 22.11, (2010) 112113.
- [23] E. Keita, S. A. Koehler, P. Faure, D. A. Weitz, and P. Coussot, Drying kinetics driven by the shape of the air/water interface in a capillary channel. *European Physical Journal E--Soft Matter*, 39(2), 2016.
- [24] J. C. T. Eijkel, B. Dan, H. W. Reemeijer, D. C. Hermes, J. G. Bomer, and A. van den Berg, Strongly accelerated and humidity-independent drying of nanochannels induced by sharp corners, *Phys. Rev. Lett.*, 95, 256107 (2005).
- [25] H. M. Princen, Capillary phenomena in assemblies of parallel cylinders: I. Capillary rise between two cylinders, *Journal of Colloid and Interface Science*, 30.1, (1969) 69.
- [26] H. M. Princen, Capillary phenomena in assemblies of parallel cylinders: II. Capillary rise in systems with more than two cylinders, *Journal of Colloid and Interface Science*, 30.3, (1969) 359.
- [27] D. Or, P. Lehmann, E. Shabraeni, and N. Shokri, Advances in soil evaporation physics — A review, *Vadose Zone Journal* 12.4 (2013).
- [28] H. M. Princen, Capillary phenomena in assemblies of parallel cylinders: III. Liquid columns between horizontal parallel cylinders, *Journal of Colloid and Interface Science*, 34.2, (1970) 171.
- [29] M. Aminzadeh and D. Or, Energy partitioning dynamics of drying terrestrial surfaces, *Journal of hydrology*, 519, (2014) 1257-1270.
- [30] E. Haghighi and D. Or, Thermal signatures of turbulent airflows interacting with evaporating thin porous surfaces, *International Journal of Heat and Mass Transfer*, 87, (2015) 429-446.
- [31] M. Aminzadeh, D. Breitenstein, and D. Or, Characteristics of Turbulent Airflow Deduced from Rapid Surface Thermal Fluctuations: An Infrared Surface Anemometer, *Boundary-Layer Meteorology*, (2017) 1-16.
- [32] M. Aminzadeh and D. Or, Pore-scale study of thermal fields during evaporation from drying porous surfaces. *International Journal of Heat and Mass Transfer*, 104, (2017) 1189-1201.
- [33] M. Suzuki and S. Maeda, On the mechanism of drying of granular beds, *Journal of chemical engineering of Japan*, 1(1), (1968) 26-31.
- [34] E. U. Schlünder, On the mechanism of the constant drying rate period and its relevance to diffusion controlled catalytic gas phase reactions, *Chemical Engineering Science*, 43(10), (1988) 2685-2688.
- [35] M. J. Stefan, Über die Verdampfung aus einem kreisförmig oder elliptisch begrenzten Becken. - *Sitzungsber. Kais. Akad. Wiss., Wien. Mathem. - naturwiss., CI. II, LXXXIII*, p. 943 (1881).
- [36] H. T. Brown and F. Escombe, Static diffusion of gases and liquids in relation to the assimilation of carbon and translocation in plants, *Proceedings of the Royal Society of London*, 67(435-441), (1900) 124-128.
- [37] G. G. J. Bange, On the quantitative explanation of stomatal transpiration, *Acta Botanica Neerlandica*, 2(3), (1953) 255-297.
- [38] J. R. Lloyd and W. R. Moran, Natural convection adjacent to horizontal surface of various planforms, *Journal of Heat Transfer* 96, no. 4 (1974): 443-447.